Article

Anticancer and Antimicrobial Metallopharmaceutical Agents Based on Palladium, Gold, and Silver N-Heterocyclic Carbene Complexes

Sriparna Ray, Renu Mohan, Jay K. Singh, Manoja K. Samantaray, Mobin M. Shaikh, Dulal Panda, and Prasenjit Ghosh

J. Am. Chem. Soc., **2007**, 129 (48), 15042-15053 • DOI: 10.1021/ja075889z

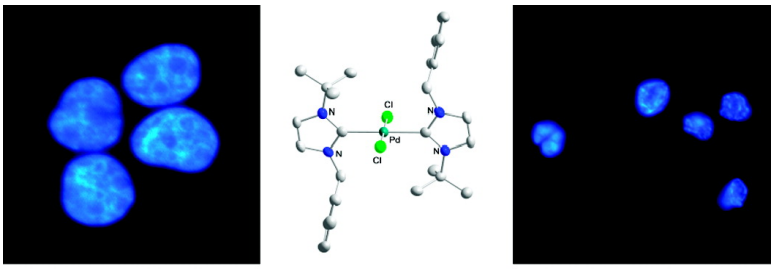

More About This Article

Additional resources and features associated with this article are available within the HTML version:

- Supporting Information
- Links to the 22 articles that cite this article, as of the time of this article download
- Access to high resolution figures
- Links to articles and content related to this article
- Copyright permission to reproduce figures and/or text from this article

View the Full Text HTML

J|A|C|S
ARTICLES
Published on Web 11/08/2007

Anticancer and Antimicrobial Metallopharmaceutical Agents Based on Palladium, Gold, and Silver N-Heterocyclic Carbene Complexes

Sriparna Ray,[†] Renu Mohan,[⊥] Jay K. Singh,[⊥] Manoja K. Samantaray,[†] Mobin M. Shaikh,[§] Dulal Panda,*[,⊥] and Prasenjit Ghosh*[,†]

Contribution from the Department of Chemistry, School of Biosciences and Bioengineering, and National Single Crystal X-ray Diffraction Facility, Indian Institute of Technology Bombay, Powai, Mumbai 400 076, India

Received August 6, 2007; E-mail: panda@iitb.ac.in; pghosh@chem.iitb.ac.in

Abstract: Complete synthetic, structural, and biomedical studies of two Pd complexes as well as Au and Ag complexes of 1-benzyl-3-*tert*-butylimidazol-2-ylidene are reported. Specifically, *trans*-[1-benzyl-3-*tert*-butylimidazol-2-ylidene]Pd(pyridine)Cl_2 (**1a**) was synthesized from the reaction of 1-benzyl-3-*tert*-butylimidazolium chloride (**1**) with $PdCl_2$ in the presence of K_2CO_3 as a base. The other palladium complex, [1-benzyl-3-*tert*-butylimidazol-2-ylidene]$_2PdCl_2$ (**1b**), and a gold complex, [1-benzyl-3-*tert*-butylimidazol-2-ylidene]AuCl (**1c**), were synthesized by following a transmetallation route from the silver complex, [1-benzyl-3-*tert*-butylimidazol-2-ylidene]AgCl (**1d**), by treatment with (COD)$PdCl_2$ and (SMe_2)AuCl, respectively. The silver complex **1d** in turn was synthesized by the reaction of **1** with Ag_2O. The molecular structures of **1a**−**d** have been determined by X-ray diffraction studies. Biomedical studies revealed that, while the palladium complexes **1a** and **1b** displayed potent anticancer activity, the gold (**1c**) and silver (**1d**) complexes exhibited significant antimicrobial properties. Specifically, **1b** showed strong antiproliferative activity against three types of human tumor cells, namely, cervical cancer (HeLa), breast cancer (MCF-7), and colon adenocarcinoma (HCT 116), in culture. The antiproliferative activity of **1b** was found to be considerably stronger than that of cisplatin. The **1b** complex inhibited tumor cell proliferation by arresting the cell cycle progression at the G2 phase, preventing the mitotic entry of the cell. We present evidence suggesting that the treated cells underwent programmed cell death through a p53-dependent pathway. Though both the gold (**1c**) and silver (**1d**) complexes showed antimicrobial activity toward *Bacillus subtilis*, **1c** was found to be ca. 2 times more potent than **1d**.

Introduction

With metallopharmaceuticals playing a significant role in therapeutic and diagnostic medicine, the discovery and development of new metallodrugs remain an ever-growing area of research in medicinal inorganic chemistry.[1] The much-familiar cisplatin, *cis*-$(NH_3)_2PtCl_2$, along with its second-generation analogue, carboplatin, are still among the most widely used chemotherapeutic agents worldwide today.[2] However, cisplatin displays several limitations that restrict its utility to a great extent. For example, cisplatin is effective only for a narrow spectrum of tumor cells and additionally, because of its poor aqueous solubility (1 mg/mL), is administered intravenously.[3] Moreover, the various toxicity issues like nephrotoxicity, neurotoxicity, emetogenesis, etc., associated with cisplatin, further complicate its usage.[3] Last, the resistance of tumor cells toward cisplatin, both natural and gradually acquired during the treatment, seriously undermines its utility.[2b,4] Thus, with the emergence of many exciting biomedical applications of various other transition metals spanning anticancer[5] to antimicrobial[6] to antifungal activities,[7] the focus is gradually shifting beyond Pt lately.[8]

[†] Department of Chemistry.
[⊥] School of Biosciences and Bioengineering.
[§] National Single Crystal X-ray Diffraction Facility.

(1) (a) Mascini, M.; Bagni, G.; Pietro, M. L. D.; Ravera, M.; Baracco, S.; Osella, D. *BioMetals* **2006**, *19*, 409−418. (b) Kostova, I. *Recent Pat. Anti-Cancer Drug Discovery* **2006**, *1*, 1−22. (c) Farver, O. *Textbook of Drug Design and Discovery*, 3rd ed.; Taylor & Francis Ltd.: London, UK, 2002; pp 364−409. (d) Guo, Z.; Sadler, P. J. *Advances in Inorganic Chemistry*; Academic Press: San Diego, 2000; Vol. 49, pp 183−306.
(2) (a) Fuertes, M. A.; Alonso, C.; Pérez, J. M. *Chem. Rev.* **2003**, *103*, 645−662. (b) Giese, B.; Deacon, G. B.; Kuduk-Jaworska, J.; McNaughton, D. *Biopolymers (Biospectroscopy)* **2002**, *67*, 294−297. (c) Jamieson, E. R.; Lippard, S. J. *Chem. Rev.* **1999**, *99*, 2467−2498.
(3) (a) Gianomenico, C.; Christen, M. U.S. Patent 6413953, 2000. (b) Lippert, B. *Cisplatin: Chemistry and Biochemistry of a Leading Anticancer Drug*; Wiley-VCH: Weinheim, 1999. (c) Lippard, S. J. *Progress in Inorganic Chemistry: Bioinorganic Chemistry*; Wiley: Sydney, 1995; Vol. 48.
(4) (a) Marzano, C.; Sbovata, S. M.; Bettio, F.; Michelin, R. A.; Seraglia, R.; Kiss, T.; Venzo, A.; Bertani, R. *J. Biol. Inorg. Chem.* **2007**, *12*, 477−493. (b) Siddik, Z. H. *Oncogene* **2003**, *22*, 7265−7279.
(5) (a) Henderson, W.; Nicholson, B. K.; Tiekink, E. R. T. *Inorg. Chim. Acta* **2006**, *359*, 204−214. (b) Quiroga, A. G.; Ranninger, C. N. *Coord. Chem. Rev.* **2004**, *248*, 119−133. (c) Goss, C. H. A.; Henderson, W.; Wilkins, A. L.; Evans, C. *J. Organomet. Chem.* **2003**, *679*, 194−201.
(6) (a) Gottschaldt, M.; Pfeifer, A.; Koth, D.; Görls, H.; Dahse, H.-M.; Möllmann, U.; Obatad, M.; Yano, S. *Tetrahedron* **2006**, *62*, 11073−11080. (b) Noguchi, R.; Hara, A.; Sugie, A.; Nomiya, K. *Inorg. Chem. Commun.* **2006**, *9*, 355−359. (c) Nomiya, K.; Yamamoto, S.; Noguchi, R.; Yokoyama, H.; Kasuga, N. C.; Ohyama, K.; Kato, C. *J. Inorg. Biochem.* **2003**, *95*, 208−220. (d) Nomiya, K.; Noguchi, R.; Ohsawa, K.; Tsuda, K.; Oda, M. *J. Inorg. Biochem.* **2000**, *78*, 363−370. (e) Nomiya, K.; Noguchi, R.; Oda, M. *Inorg. Chim. Acta* **2000**, *298*, 24−32.

 10.1021/ja075889z CCC: $37.00

Displaying structural preferences similar to those of Pt and also exhibiting promising cytotoxicity, Pd naturally qualifies for metallodrugs, a notion progressively gaining credence in the light of new information emerging lately.[9] Quite interestingly, the *trans*-L_2PdCl_2-type complexes have been found to exhibit higher cytotoxicity than their *cis*-platinum analogues, *cis*-L_2PtCl_2, for the same ligand system (L = dimethyl 5-(2-hydroxyphenyl)-1,3-dimethyl-1*H*-pyrazol-4-ylphosphonate and methyl 5-(2-hydroxyphenyl)-1,3-dimethyl-1*H*-pyrazole-4-carboxylate).[9a,10] In this context, it is also worth noting that several Pd complexes, namely, $[(RO)CS_2]_2Pd$ (R = Et, *i*-Pr, Cy), have been reported to display favorable cytotoxicity at pH 6.8, a condition common in tumor cells, whereas the pH of normal cells is 7.4.[9c] Moreover, hydrolytic and DNA-binding studies on the Pd(II) and Pt(II) complexes with anticancer activities showed that the palladium complexes are kinetically labile, produce new charged species to interact with DNA, and also bind to DNA at a faster rate than the platinum complexes.[11] Subscribing to a similar point of view, we decided to explore the potential of palladium complexes as anticancer agents.

The success of metallodrugs is, however, closely interlinked with the proper choice of the ancillary ligands, as they play a crucial role in modifying reactivity and lipophilicity, in stabilizing specific oxidation states, in imparting substitution inertness, and in suppressing the adverse effect of the metal ion in order to facilitate positive impacts in the areas of diagnosis and therapy.[12] The biomedical applications of metal complexes based on N-heterocyclic carbene (NHC)[13−15] are just beginning to unfold, despite such complexes being phenomenally successful in homogeneous catalysis.[16] As our research objective is in design and utility of NHC−metal complexes,[17] we became interested in exploring the potentials of Pd−, Au−, and Ag−NHC complexes as metallopharmaceuticals. Our inspiration for the anticancer study came from a potent anticancer prodrug, *trans*-$(pyridine)_2PtCl_2$,[18] modeled on which we set out to design a series of Pd-based complexes, *trans*-$(NHC)_nPd(pyridine)_mCl_2$ (n = 1, 2 and m = 1, 0 respectively), in which the pyridine moiety is sequentially replaced by a more electron-donating NHC ligand.[17f,g,19] Such a study assumes relevance in the absence of any prior report available on Pd−NHC complexes in anticancer studies, though Pd−pyridine[20] and Pd−amine[21] complexes are known to show considerable antiproliferative properties against tumor cells.

Our impetus for the antimicrobial study came from the knowledge that elemental silver and its salts are long known for their antimicrobial properties, particularly against chronic ulcers, extensive burns, and difficult-to-heal wounds.[13d] The activity of silver is predominantly due to its interference with the electron transport system of the cell, its interaction with the cell membrane, and its interaction with thiol groups of the vital enzymes of bacteria.[22] The primary challenge in designing silver-based antimicrobial agents lies in the slow and sustained release of Ag ions over a period of time in the affected area. In this regard, it is worth mentioning that Youngs and co-workers[13b] recently reported Ag−NHC complexes, namely, $[L_2Ag_2]\ 2(X^-)$ [L = $C_{18}N_5O_2$ (imidazol-2-ylidene cyclophane *gem*-diol-type ligand), X = OH^-, CO_3^{2-}], embedded in a polymer matrix that showed significant antimicrobial activity. In contrast to silver, however, gold displays a varied range of biomedical applications, spanning antiarthritic[23] to antitumor[14] to antimicrobial activities.[13] N-Heterocyclic carbenes, being extremely good σ-donor ligands, form strong Au−C_{carb} bonds, thereby making stable Au−NHC complexes that are not susceptible to biologi-

(7) (a) Coyle, B.; McCann, M.; Kavanagh, K.; Devereux, M.; McKee, V.; Kayal, N.; Egan, D.; Deegan, C.; Finn, G. J. *J. Inorg. Biochem.* **2004**, *98*, 1361−1366. (b) Abuskhuna, S.; Briody, J.; McCann, M.; Devereux, M.; Kavanagh, K.; Fontecha, J. B.; McKee, V. *Polyhedron* **2004**, *23*, 1249−1255. (c) Tsyba, I.; Mui, B. B.; Bau, R.; Noguchi, R.; Nomiya, K. *Inorg. Chem.* **2003**, *42*, 8028−8032. (d) Coyle, B.; Kavanagh, K.; McCann, M.; Devereux, M.; Geraghty, M. *BioMetals* **2003**, *16*, 321−329. (e) Dinger, M. B.; Henderson, W. *J. Organomet. Chem.* **1998**, *560*, 233−243.

(8) Clarke, M. J.; Zhu, F.; Frasca, D. R. *Chem. Rev.* **1999**, *99*, 2511−2533.

(9) (a) Navarro, M.; Peña, N. P.; Colmenares, I.; González, T.; Arsenak, M.; Taylor, P. *J. Inorg. Biochem.* **2006**, *100*, 152−157. (b) Friaza, G. G.; Fernández-Botello, A.; Pérez, J. M.; Prieto, M. J.; Moreno, V. *J. Inorg. Biochem.* **2006**, *100*, 1368−1377. (c) Friebolin, W.; Schilling, G.; Zöller, M.; Amtmann, E. *J. Med. Chem.* **2005**, *48*, 7925−7931. (d) Guo, Z.; Sadler, P. J. *Angew. Chem., Int. Ed.* **1999**, *38*, 1512−1531. (e) Puthraya, K. H.; Srivastava, T. S.; Amonkar, A. J.; Adwankar, M. K.; Chitnis, M. P. *J. Inorg. Biochem.* **1985**, *25*, 207−215.

(10) Budzisz, E.; Krajewska, U.; Rozalski, M.; Szulawska, A.; Czyz, M.; Nawrot, B. *Eur J. Pharm.* **2004**, *502*, 59−65.

(11) González, M. L.; Tercero, J. M.; Matilla, A.; Niclós-Gutiérrez, J.; Fernández, M. T.; López, M. C.; Alonso, C.; González, S. *Inorg. Chem.* **1997**, *36*, 1806−1812.

(12) Storr, T.; Thompson, K. H.; Orvig, C. *Chem. Soc. Rev.* **2006**, *35*, 534−544.

(13) (a) Kascatan-Nebioglu, A.; Melaiye, A.; Hindi, K.; Durmus, S.; Panzner, M. J.; Hogue, L. A.; Mallett, R. J.; Hovis, C. E.; Coughenour, M.; Crosby, S. D.; Milsted, A.; Ely, D. L.; Tessier, C. A.; Cannon, C. L.; Youngs, W. J. *J. Med. Chem.* **2006**, *49*, 6811−6818. (b) Melaiye, A.; Sun, Z.; Hindi, K.; Milsted, A.; Ely, D.; Reneker, D. H.; Tessier, C. A.; Youngs, W. J. *J. Am. Chem. Soc.* **2005**, *127*, 2285−2291. (c) Garrison, J. C.; Tessier, C. A.; Youngs, W. J. *J. Organomet. Chem.* **2005**, *690*, 6008−6020. (d) Melaiye, A.; Simons, R. S.; Milstead, A.; Pingitore, F.; Wesdemiotis, C.; Tessier, C. A.; Youngs, W. J. *J. Med. Chem.* **2004**, *47*, 973−977.

(14) (a) Barnard, P. J.; Wedlock, L. E.; Baker, M. V.; Berners-Price, S. J.; Joyce, D. A.; Skelton, B. W.; Steer, J. H. *Angew. Chem., Int. Ed.* **2006**, *45*, 5966−5970. (b) Baker, M. V.; Barnard, P. J.; Berners-Price, S. J.; Brayshaw, S. K.; Hickey, J. L.; Skelton, B. W.; White, A. H. *Dalton Trans.* **2006**, 3708−3715. (c) Barnard, P. J.; Baker, M. V.; Berners-Price, S. J. *J. Inorg. Biochem.* **2004**, *98*, 1642−1647.

(15) Özdemir, I.; Denizci, A.; Öztürk, H. T.; Çetinkaya, B. *Appl. Organomet. Chem.* **2004**, *18*, 318−322.

(16) (a) Lin, I. J. B.; Vasam, C. S. *Coord. Chem. Rev.* **2007**, *251*, 642−670. (b) Garrison, J. C.; Youngs, W. J. *Chem. Rev.* **2005**, *105*, 3978−4008. (c) Peris, E.; Crabtree, R. H *Coord. Chem. Rev.* **2004**, *248*, 2239−2246. (d) Arnold, P. L. *Heteroat. Chem.* **2002**, *13*, 534−539. (e) Herrmann, W. A. *Angew. Chem., Int. Ed.* **2002**, *41*, 1290−1309.

(17) (a) Ray, L.; Shaikh, M. M.; Ghosh, P. *Dalton Trans.* **2007**, 4546-4555. (b) Ray, L.; Katiyar, V.; Barman, S.; Raihan, M. J.; Nanavati, H.; Shaikh, M. M.; Ghosh, P. *J. Organomet. Chem.* **2007**, *692*, 4259−4269. (c) Samantaray, M. K.; Katiyar, V.; Pang, K.; Nanavati, H.; Ghosh, P. *J. Organomet. Chem.* **2007**, *692*, 1672−1682. (d) Ray, L.; Shaikh, M. M.; Ghosh, P. *Organometallics* **2007**, *26*, 958−964. (e) Ray, L.; Katiyar, V.; Raihan, M.; Nanavati, H.; Shaikh, M. M.; Ghosh, P. *Eur. J. Inorg. Chem.* **2006**, *3724−3730*. (f) Samantaray, M. K.; Roy, D.; Patra, A.; Stephen, R.; Saikh, M.; Sunoj, R. B.; Ghosh, P. *J. Organomet. Chem.* **2006**, *691*, 3797−3805. (g) Samantaray, M. K.; Katiyar, V.; Roy, D.; Pang, K.; Nanavati, H.; Stephen, R.; Sunoj, R. B.; Ghosh, P. *Eur. J. Inorg. Chem.* **2006**, 2975−2984.

(18) (a) Ghezzi, A. R.; Aceto, M.; Cassino, C.; Gabano, E.; Osella, D. *J. Inorg. Biochem.* **2004**, *98*, 73−78. (b) Colangelo, D.; Ghiglia, A. L.; Viano, I.; Mahboobi, H.; Ghezzi, A. R.; Cassino, C.; Osella, D. *J. Inorg. Biochem.* **2004**, *98*, 61−67. (c) Beusichem, M. V.; Farrell, N. *Inorg. Chem.* **1992**, *31*, 634−639.

(19) (a) Nemcsok, D.; Wichmann, K.; Frenking, G. *Organometallics* **2004**, *23*, 3640−3646. (b) Boehme, C.; Frenking, G. *Organometallics* **1998**, *17*, 5801−5809.

(20) (a) Kovala-Demertzi, D.; Boccarelli, A.; Demertzis, M. A.; Coluccia, M. *Chemotherapy* **2007**, *53*, 148−152. (b) Kovala-Demertzi, D.; Demertzis, M. A.; Filiou, E.; Pantazaki, A. A.; Yadav, P. N.; Miller, J. R.; Zheng, Y.; Kyriakidis, D. A. *BioMetals* **2003**, *16*, 411−418. (c) Kuduk-Jaworska, J.; Puszko, A.; Kubiak, M.; Pełczyñska, M. *J. Inorg. Biochem.* **2004**, *98*, 1447−1456. (d) Zhao, G.; Lin, H.; Yu, P.; Sun, H.; Zhu, S.; Su, X.; Chen, Y. *J. Inorg. Biochem.* **1999**, *73*, 145−149. (e) Kovala-Demertzi, D.; Millerb, J. R.; Kourkoumelisa, N.; Hadjikakoua, S. K.; Demertzis, M. A. *Polyhedron* **1999**, *18*, 1005−1013.

(21) (a) Ruiz, J.; Cutillas, N.; Vicente, C.; Villa, M. D.; López, G. *Inorg. Chem.* **2005**, *44*, 7365−7376. (b) Abu-Surrah, A. S.; Al-Allaf, T. A. K.; Rashan, L. J.; Klinga, M.; Leskelä, M. *Eur. J. Med. Chem.* **2002**, *37*, 919−922. (c) Faraglia, G.; Fregona, D.; Sitranb, S.; Giovagninia, l.; Marzanoc, C.; Baccichetti, F.; Casellato, U.; Graziani, R. *J. Inorg. Biochem.* **2001**, *83*, 31−40. (d) Suvachittanont, S.; Hohmann, H.; van Eldik, R.; Reedijk, J. *Inorg. Chem.* **1993**, *32*, 4544−4548.

(22) Kasuga, N. C.; Sugie, A.; Nomiya, K. *Dalton Trans.* **2004**, 3732−3740.

(23) (a) Gunatilleke, S. S.; Barrios, A. M. *J. Med. Chem.* **2006**, *49*, 3933−3937. (b) Talib, J.; Beck, J. L.; Ralph, S. F. *J. Biol. Inorg. Chem.* **2006**, *11*, 559−570. (c) Chicorian, A.; Barrios, A. M. *Bioorg. Med. Chem. Lett.* **2004**, *14*, 5113−5116.

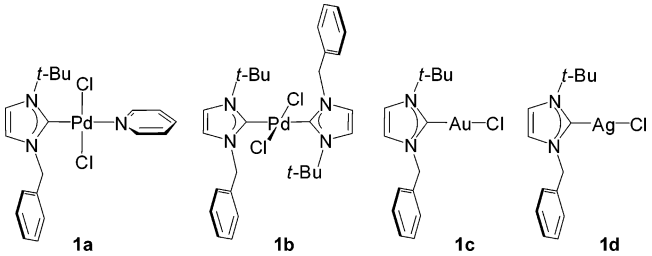

Figure 1. Structures of compounds **1a**−**d**.

cally important thiol groups.[15] Thus, keeping with our objective of exploring the biomedical applications of transition metal complexes of NHCs, we decided to synthesize Au− and Ag−NHC complexes and study their antimicrobial properties.

In this contribution, we report the synthesis, structure, and biomedical applications of a series of transition metal−NHC complexes. In particular, we report two Pd complexes, (NHC)-Pd(pyridine)Cl_2 (**1a**) and $(NHC)_2PdCl_2$ (**1b**), that display strong cytotoxicity against three different types of human tumor cell lines in culture and Au and Ag complexes, (NHC)MCl [M = Au (**1c**), Ag (**1d**)], that exhibit significant antimicrobial activities (Figure 1).

Results and Discussion

Two palladium complexes of the type *trans*-$(NHC)_n$Pd-$(pyridine)_mCl_2$ ($n = m = 1$, **1a**; $n = 2$, $m = 0$, **1b**) and gold and silver complexes of the type (NHC)MCl (M = Au, **1c**; Ag, **1d**], stabilized over a N-heterocyclic ligand, namely, 1-benzyl-3-*tert*-butylimidazol-2-ylidene, were synthesized for the purpose of biomedical application studies. It is worth mentioning that the two *trans*-$(NHC)_n$Pd$(pyridine)_mCl_2$ complexes **1a** and **1b** were, however, synthesized using different pathways: **1a** was synthesized by a direct reaction of 1-benzyl-3-*tert*-butylimidazolium chloride (**1**) with $PdCl_2$ in pyridine, while **1b** was obtained from the silver complex **1d** by treatment with (COD)-$PdCl_2$, employing a frequently used carbene-transfer route[24] (Scheme 1). Formations of **1a** and **1b** was confirmed by the appearance of the diagnostic metal-bound carbene (N*C*N−Pd) resonances at 151.4 ppm (**1a**) and 166.9 ppm (**1b**) in their respective $^{13}C\{^1H\}$ NMR spectrum, and these values are well within the range (175−145 ppm) observed in other Pd−NHC complexes.[25] The *tert*-butyl moiety $-C(CH_3)_3$ appeared as a singlet at 2.12 ppm (**1a**) and 1.98 ppm (**1b**) in the respective ^1H NMR spectrum, as expected.

The molecular structures of **1a** and **1b** have been determined by X-ray diffraction studies, which showed that both metal centers were in square-planar geometries (see Supporting Information, Figures S1 and S2). The Pd−C(carbene) bond distances of 1.955(2) Å in **1a** and 2.044(4) Å in **1b** are comparable to the sum of individual covalent radii of Pd and C (Pd−C = 2.055 Å)[26] and are in agreement with those observed in other Pd−NHC complexes.[27] It is worth noting that the metal-bound pyridine in the (NHC)Pd(pyridine)Cl_2 (**1a**) structure was found to be tilted (torsion angle C19−N3−C1−N1) by 53.3° relative to the plane containing the imidazolium ring of the NHC ligand. The Pd−N(pyridine) distance of 2.1098(19) Å in **1a** is longer than the sum of the individual covalent radii of Pd and N (Pd−N = 1.983 Å)[26] but closely resembles those observed in related analogues, [1,3-bis-2,6-di-isopropylphenyl-imidazol-2-ylidene]$PdCl_2$(3-chloropyridine) [2.137(2) Å][28] and [1-benzyl-3-(*N*-phenylacetamide)-imidazol-2-ylidene]Pd(pyridine)Cl_2 [2.073-(2) Å].[29] The longer Pd−N(pyridine) distance in **1a** is attributed to the greater *trans* effect[30] of the NHC ligand residing diagonally opposite to the pyridine. As anticipated, for the $(NHC)_2PdCl_2$ complex **1b**, the two NHC ligands were in *trans* disposition to each other around the palladium center. Furthermore, the imidazolium rings of the two NHC ligands were coplanar. It is worth mentioning that the coplanarity of imidazolium rings observed in **1b** is not unusual and has been observed in other *trans*-$(NHC)_2PdCl_2$-type complexes, including [1-(*o*-methoxybenzyl)-3-*tert*-butylimidazol-2-ylidene]$_2$-$PdCl_2$,[17d] [1-(*tert*-butyl)-3-{*N*-phenol}-imidazol-2-ylidine]$_2PdCl_2$,[31] [1-(methyl)-3-{*N*-(2,6-di-isopropylphenylimino)-2-phenylethyl}-imidazol-2-ylidine]$_2PdCl_2$,[32] and [*N*-benzylidene-2-(1-isopropyl-4-phenyl-imidazol-2-ylidene) cyclohexanamine]$_2PdCl_2$.[33] Also, the N-1 (benzyl) and N-3 (*tert*-butyl) substituents on the imidazolium ring of one NHC ligand are oriented *trans* to the respective N-1 and N-3 substituents of the other NHC ligand in the **1b** structure. The Pd−Cl distances in **1a** [2.3114(6) Å] and **1b** [2.3268(10) Å] are comparable to each other.

The gold complex **1c** was synthesized analogously following the carbene-transfer route from the reaction of the silver complex **1d** with (SMe_2)AuCl. The $^{13}C\{^1H\}$ NMR spectrum showed the diagnostic Au−C(carbene) peak at 169.2 ppm, similar to what is observed for analogous Au−NHC complexes, e.g., 169.2 ppm in [1-(*o*-methoxybenzyl)-3-(*tert*-butyl)imidazol-2-ylidene]AuCl[17d] and 170.2 ppm in [3-(*N*-*tert*-butylacetamido)-1-(2-hydroxycyclohexyl)imidazol-2-ylidene]AuCl.[17e] The high-resolution electrospray mass spectrometry (HRMS) data of **1c** showed a peak at *m*/*z* 411.1143, corresponding to the cationic fragment {[1-benzyl-3-*tert*-butylimidazol-2-ylidene]Au}$^+$ (calculated *m*/*z* 411.1136).

(24) Wang, H. M. J.; Lin, I. J. B. *Organometallics* **1998**, *17*, 972−975.
(25) (a) Gründemann, S.; Albrecht, M.; Loch, J. A.; Faller, J W.; Crabtree, R. H. *Organometallics* **2001**, *20*, 5485−5488. (b) Herrmann, W. A.; Bohm, V. P. W.; Gstottmayr, C. W. K.; Grosche, M.; Reisinger, C.-P.; Weskamp, T. *J. Organomet. Chem.* **2001**, *617*−*618*, 616−628. (c) Herrmann, W. A.; Schwarz, J.; Gardiner, M. G.; Spiegler, M. *J. Organomet. Chem.* **1999**, *575*, 80−86. (d) Gardiner, M. G.; Herrmann, W. A.; Reisinger, C.-P.; Schwarz, J.; Spiegler, M. *J. Organomet. Chem.* **1999**, *572*, 239−247.
(26) Pauling, L. *The Nature of the Chemical Bond*, 3rd ed.; Cornell University Press: Ithaca, NY, 1960; pp 224−228.
(27) (a) Bertogg, A.; Campanovo, F.; Togni, A. *Eur. J. Inorg. Chem.* **2005**, 347−356. (b) Frey, G. D.; Schütz, J.; Herdtweck, E.; Herrmann, W. A. *Organometallics* **2005**, *24*, 4416−4426. (c) Tulloch, A. A. D.; Winston, S.; Danopoulos, A. A.; Eastham, G.; Hursthouse, M. B. *Dalton Trans.* **2003**, 699−708. (d) Loch, J. A.; Albrecht, M.; Peris, E.; Mata, J.; Faller, J. W.; Crabtree, R. H. *Organometallics* **2002**, *21*, 700−706. (e) Douthwaite, R. E.; Green, M. L. H.; Silcock P. J.; Gomes, P. T. *J. Chem. Soc., Dalton Trans.* **2002**, 1386−1390. (f) Magill, A. M.; McGuinness, D. S.; Cavell, K. J.; Britovsek, G. J. P.; Gibson, V. C.; White, A. J. P.; Williams, D. J.; White, A. H.; Skelton, B. W. *J. Organomet. Chem.* **2001**, *617*−618, 546−560. (g) Tulloch, A. A. D.; Danopoulos, A. A.; Tooze, R. P.; Cafferkey, S. M.; Kleinhenz, S.; Hursthouse, M. B. *Chem. Commun.* **2000**, 1247−1248.
(28) O'Brien, C. J.; Kantchev, E. A. B.; Valente, C.; Hadei, N.; Chass, G. A.; Lough, A.; Hopkinson, A. C.; Organ, M. G. *Chem. Eur. J.* **2006**, *12*, 4743−4748.
(29) Liao, C.-Y.; Chan, K.-T.; Zeng, J.-Y.; Hu, C.-H.; Tu, C.-Y.; Lee, H. M. *Organometallics* **2007**, *26*, 1692−1702.
(30) (a) Dragutan, V.; Dragutan, I. *Platinum Metals Rev.* **2005**, *49*, 183−188. (b) Guerra, G. *Synlett* **2003**, *3*, 423−424. (c) Duan, W.-L.; Shi, M.; Rong, G.-B. *Chem. Commun.* **2003**, 2916−2917. (d) Gründemann, S.; Albrecht, M.; Kovacevic, A.; Faller, J. W.; Crabtree, R. H. *J. Chem. Soc., Dalton Trans.* **2002**, 2163−2167. (e) Sanford, M. S.; Love, J. A.; Grubbs, R. H. *J. Am. Chem. Soc.* **2001**, *123*, 6543−6554. (f) McGuinness, D. S.; Cavell, K. J.; Yates, B. F.; Skelton, B. W.; White, A. H. *J. Am. Chem. Soc.* **2001**, *123*, 8317−8328.
(31) Boydston, A. J.; Rice, J. D.; Sanderson, M. D.; Dykhno, O. L.; Bielawski, C. W. *Organometallics* **2006**, *25*, 6087−6098.
(32) Frøseth, M.; Netland, K. A.; Tõrnroos, H. W.; Dhindsa, A.; Tilset, *Dalton Trans.* **2005**, 1664−1674.
(33) Bonnet, L. G.; Douthwaite, R. E.; Hodgson, R.; Houghton, J.; Kariuki, B. M.; Simonovic, S. *Dalton Trans.* **2004**, 3528−3535.

Scheme 1

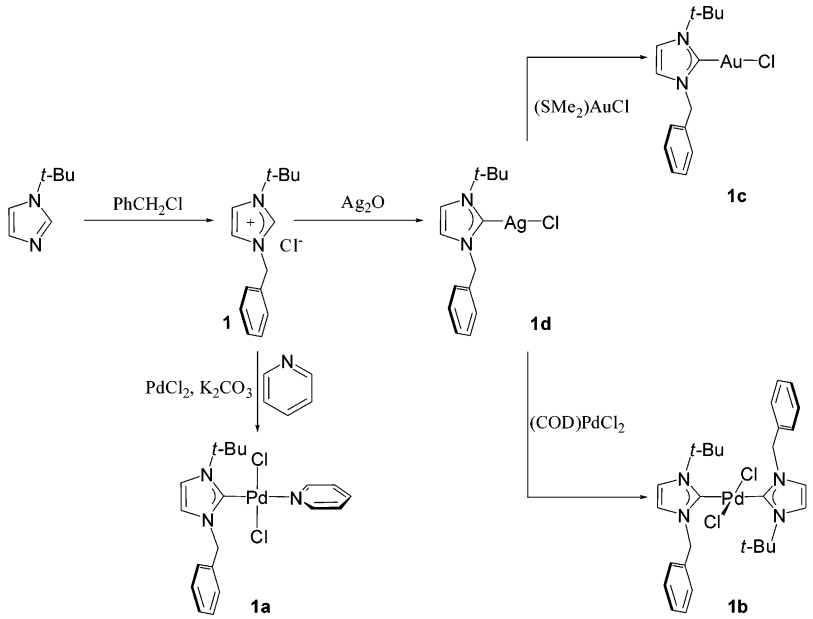

The silver complex **1d** was synthesized by the treatment of the 1-benzyl-3-*tert*-butylimidazolium chloride salt (**1**) with Ag_2O.[24] The ^1H NMR spectrum of the **1d** showed the absence of the downfield-shifted NC*H*N resonance in the 10 ppm region, indicating the deprotonation of the acidic proton of **1**, in accordance with the formation of **1d**. The $^{13}C\{^1H\}$ NMR spectrum further confirmed the formation of **1d**, as the N*C*N−Ag resonance appeared highly downfield-shifted at 177.7 ppm. The benzyl methylene (−CH_2−) peak appeared at 5.34 ppm in the ^1H NMR spectrum and at 56.7 ppm in the $^{13}C\{^1H\}$ NMR spectrum.

The solid-state structure analyses of gold (**1c**) and silver (**1d**) complexes[34] showed significant differences (see Supporting Information, Figures S3 and S4). While the gold complex **1c** was found to be monomeric with a linear geometry at the metal center [∠C1−Au1−Cl1 = 178.88(17)°], the silver complex **1d** exhibited a dimeric structure having a bent angle [∠C1−Ag1−Cl1 = 154.40(9)°] at silver and containing a Ag_2Cl_2 core displaying two inequivalent Ag−Cl bond distances [2.4283(8) and 2.7843(9) Å]. Such dimeric structures are not uncommon, as the Ag−NHC complexes are known for their structural diversity.[16a,b,d] Examples of related (NHC)AgCl complexes containing a similar central Ag_2Cl_2 core include {ethylene-bis-[(*N*-methyl)imidazol-2-ylidene]AgCl}$_n$ [d_{Ag-Cl} = 2.481(3), 2.719-(3) Å],[35] {[1-(methyl)-3-(*N*-(+)-methylmenthoxide)imidazol-2-ylidene]$Ag^+AgCl^-_2$}$_2$ [d_{Ag-Cl} = 2.626(6), 2.526(5) Å],[36] and {[1-(mesityl)-3-{*N*,*N*-diethylcarbomethyl}imidazol-2-ylidene]-AgCl}$_2$ [d_{Ag-Cl} = 2.099(3), 2.9071(10) Å].[37]

Quite interestingly, the Au−C(carbene) bond distance [1.984-(6) Å] observed in **1c** is shorter than the sum of the individual covalent radii of Au and C (Au−C = 2.108 Å),[26] indicative of a strong Au−NHC interaction. Additionally, the Au−C(carbene) bond distance [1.984(6) Å] in **1c** is shorter than the Ag−C(carbene) bond distance [2.110(3) Å] in **1d**, consistent with the shorter covalent radius of Au than Ag.[26] It is worth noting that the charge decomposition analysis study by Frenking[19b] had earlier suggested that shorter Au−C(carbene) bond distances in Au−NHC complexes, in general, may arise due to the occurrence of relatively greater π-back-donation [Au→C-(carbene)] in Au−NHC complexes relative to that in the Ag−NHC complexes. It is worth pointing out that the shorter Au−NHC bond distance with greater amount of π-back-donation [Au→C(carbene)] relative to silver is indicative of higher Au−NHC bond strength, leading to more stable Au−NHC complexes.

Table 1. Percent Inhibition of HeLa Cell Proliferation by Complexes **1a**−**d**

concn (μM)[a]	inhibition (%)			
	1a	**1b**	**1c**	**1d**
1	7 ± 3	7 ± 3	0.3 ± 0.6	1.3 ± 0.6
5	23 ± 4	57 ± 3	0.3 ± 0.6	1.7 ± 1.5
10	35 ± 3	85 ± 2	1.7 ± 0.6	3 ± 1.7

[a] Data are the averages of three independent experiments. **1c** (25 μM) and **1d** (25 μM) inhibited HeLa cell proliferation by 3 and 5%, respectively.

Table 2. Half-Maximal Inhibitory Concentrations (IC_{50}) of **1b** and Cisplatin, Measured Using the Sulforhodamine B Assay

compd	IC_{50} (μM)[a]		
	HeLa	HCT 116	MCF-7
1b	4 ± 0.2	0.8 ± 0.05	1 ± 3
cisplatin	8 ± 1	16 ± 3	15 ± 2

[a] Data are the averages of three independent experiments.

Quite significantly, the Pd−NHC complexes **1a** and **1b** exhibit remarkable anticancer properties (Tables 1 and 2 and Figure 2), while the respective gold (**1c**) and silver (**1d**) complexes did not show any such activity (Table 1). Specifically, the cytotoxic effect of **1b** was compared to that of cisplatin on three different human tumor cells, namely, cervical cancer

(34) No spectroscopic and structural characterization of the silver complex **1d** was provided, even though the compound has been reported: Corberán, R.; Sanaú, M.; Peris, E. *Organometallics* **2006**, *25*, 4002−4008.
(35) Lee, K. M.; Wang, H. M. J.; Lin, I. J. B. *J. Chem. Soc., Dalton Trans.* **2002**, 2852−2856.
(36) Ramírez, J.; Corberán, R.; Sanaú, M.; Peris, E. *Chem. Commun.* **2005**, 3056−3058.
(37) Tulloch, A. A. D.; Danopoulos, A. A.; Winston, S.; Kleinhenz, S.; Eastham, G. *J. Chem. Soc., Dalton Trans.* **2000**, 4499−4506.

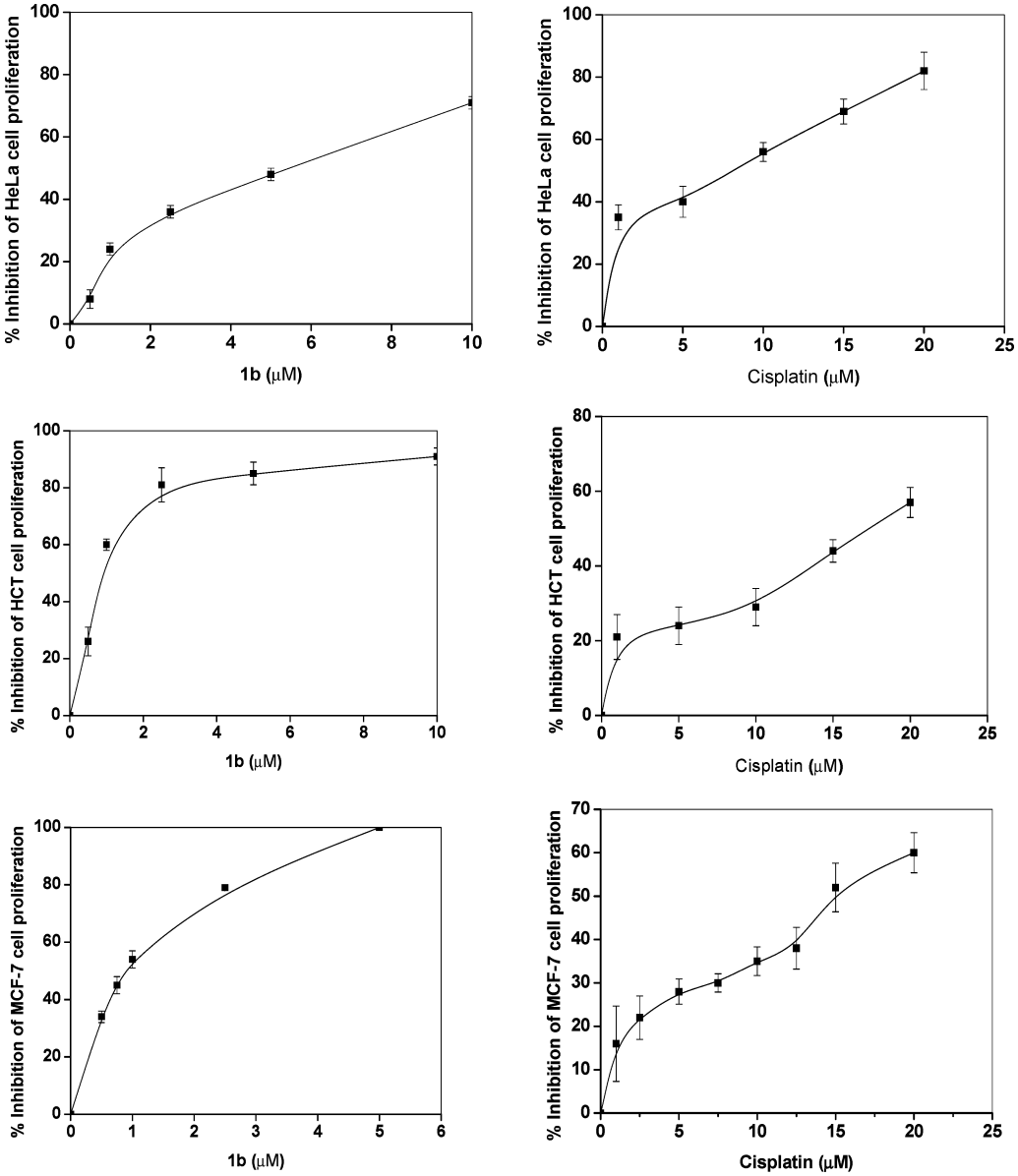

Figure 2. Inhibition of cell proliferation by **1b** and cisplatin, measured using the sulforhodamine B assay.

(HeLa), breast cancer (MCF-7), and colon adenocarcinoma (HCT 116) (Table 2). Inhibition of cell proliferation was examined by incubating cells with different concentrations of **1b** or cisplatin for one cell cycle, and the cell proliferation was measured by the standard sulforhodamine B assay.[38] **1b** potently inhibited the proliferation of HeLa, MCF-7, and HCT 116 cells in a concentration-dependent fashion (Table 2, Figure 2). Significantly enough, **1b** had a stronger inhibition effect on the proliferation of HeLa, MCF-7, and HCT 116 cells than cisplatin under similar experimental conditions (Table 2, Figure 2). Half-maximal inhibitory concentration (IC_{50}) values of cisplatin for HeLa, MCF-7, and HCT 116 were 8, 15, and 16 μM, respectively, whereas the corresponding values for **1b** were 4, 1, and 0.8 μM, respectively (Table 2). Moreover, **1b** had a stronger effect on the proliferation of MCF-7 and HCT 116 cells compared to HeLa cells. A slightly lower inhibition of HeLa cell proliferation ($35 \pm 3\%$ at 10 μM) was also observed in the case of **1a** (Table 1). The antiproliferative activities of **1a** and **1b** in culture are comparable to those of other reported organic anticancer agents, namely, noscapine ($IC_{50} = 20-35$ μM),[39] estramustine ($IC_{50} = 0.5-17$ μM),[40] and 2-methoxyestradiol ($IC_{50} = 0.4-2.5$ μM),[41] which too are active in micromolar concentrations. Interestingly enough, **1b** was found to be a more potent cytotoxic agent than the prevalent benchmark metallo-drug, cisplatin, not only under the same experimental conditions measured by us (Table 2, Figure 2) but also in comparison to the reported antiproliferative activity of cisplatin ($IC_{50} = 0.2-12$ μM).[42] The superior activity of **1b** assumes significance in light of the fact that cisplatin is undisputedly the most studied and widely used metallopharmaceutical for cancer therapy known to date.

(38) Gupta, K.; Bishop, J.; Peck, A.; Brown, J.; Wilson, L.; Panda, D. *Biochemistry* **2004**, *43*, 6645−6655.
(39) Zhou, J.; Gupta, K.; Aggarwal, S.; Aneja, R.; Chandra, R.; Panda, D.; Joshi, C. H. *Mol. Pharmacol.* **2003**, *63*, 799−807.
(40) (a) Nicholson, K. M.; Phillips, R. M.; Shnyder, S. D.; Bililey, M. C. *Eur. J. Cancer* **2002**, *38*, 194−204. (b) Sangrajrang, S.; Denoulet, P.; Laing, N. M.; Tatoud, R.; Millot, G.; Calvo, F.; Tew, K. D.; Fellows, A. *Biochem. Pharmacol.* **1998**, *55*, 325−331.
(41) Tinley, L. T.; Leal, M. R.; Randall-Hlibek, D. A.; Cessac, W. J.; Wilken, R. L.; Rao, N. P.; Mooberry, L. S. *Cancer Res.* **2003**, *63*, 1538−1549.

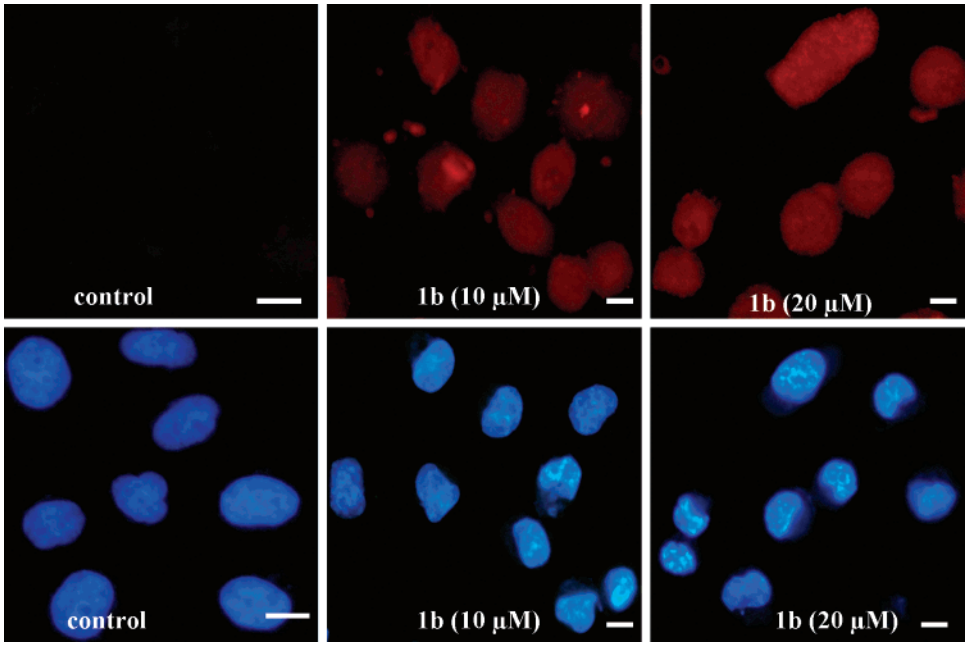

Figure 3. **1b** arrests HeLa cells at the G2−M phase of the cell cycle. Immunofluorescence images of HeLa cells in the absence and presence of 10 and 20 μM **1b** stained with anti-cyclin B1 antibody. Top panels show cells stained with antibody against cyclin B1 (red), and the lower panels show the DAPI-stained DNA of the same cells (blue). Scale bar represents 10 μm.

The observation of higher cytotoxicity in the *trans*-$(NHC)_2PdCl_2$ complex **1b**, containing two NHC ligands with strong electron-donating abilities, as compared to the (NHC)-Pd(pyridine)Cl_2 complex **1a**, containing one NHC ligand, may be correlated to the relatively more electron-rich metal center in the former. In this regard, the electron densities of the respective metal centers in **1b** and **1a** were computed using density functional theory at the B3LYP/SDD, 6-31G* level of theory, and both Mulliken and natural charge analyses showed that the Pd center in **1b** is more electron-rich than in the **1a** complex (see Supporting Information, Table S6).

Detailed mechanistic studies were undertaken on the more potent of the two, the $(NHC)_2PdCl_2$ complex **1b**, to gain insight about its mode of action, particularly its effects on the cell cycle. In order to determine the effects of **1b** on the progression of the cell cycle, HeLa cells were incubated without or with different concentrations (10 and 20 μM) of **1b** for 24 h, and then the cells were probed with antibodies against cyclin B1 and phospho-cdc2, markers of G2/M arrest. Cisplatin[43] and the related platinum compounds[44] are known to induce DNA damage and arrest the cells at the G2/M phase of the cell cycle. Progression of cells from the G2 to the M phase is regulated by cdc2 kinase and cyclin B1. Activation of cdc2 kinase occurs by the phosphorylation of Thr161,[45] whereas phosphorylation of Tyr15 and Thr14[46] is shown to inactivate cdc2 kinase. Inactivation of cdc2 by phosphorylation is mediated by Wee1 and Myt-1.[47] Kinase activity of cdc2 also requires complex formation with cyclin B1.[48] Inactive cdc2-cyclin B remains in the cytoplasm, whereas the active complex is translocated to the nucleus when the cell proceeds to mitosis from the G2 phase.[49] Therefore, we analyzed whether **1b** is able to regulate these proteins and induce cell cycle arrest. Immunofluorescence analysis of HeLa cells stained with cyclin B1 antibody revealed that **1b** caused overexpression of cyclin B1 in the cells as compared to the vehicle-treated control cells (Figure 3). Overexpression of cyclin B1 is considered to be associated with G2/M arrest and induction of apoptosis.[50] This result suggested that the **1b**-treated cells were arrested in the G2/M phase of the cell cycle. However, it was not clear whether the cells were arrested at the G2 or the M phase. To clarify this further, we used a phospho-cdc2 antibody which is specific to the G2 phase and also counted the percent of cells that were arrested at mitosis. Western blot analysis using phospho-cdc2 (Tyr-15) polyclonal antibody, specific for tyrosine 15 phosphorylation, indicated that cdc2 phosphorylation at tyrosine 15 was significantly increased in 20 μM **1b**-treated cells as compared to the vehicle-treated control, indicating that the **1b**-treated cells were arrested in the G2 phase (Figure 4). Hyperphosphorylation of cdc2 arrests the cells at the G2 phase, preventing the mitotic entry of the cells. Tyrosine phosphorylation of cdc2 has been reported in DNA damage-induced G2 cell-cycle arrest.[51,52] When the cells were stained for cyclin B1 (Figure 3), we could not detect any nuclear accumulation of cyclin B1; an increased expression of the cyclin B1 compared to the control cells was

(42) (a) Margiotta, N.; Natille, G.; Capitelli, F.; Fanizzi, P. F.; Bocarelli, A.; de Rinaldis, P.; Giordano, D.; Colucia, M. *J. Inorg. Biochem.* **2006**, *100*, 1849−1857. (b) Barbara, C.; Orlandi, P.; Bocci, G.; Fiorovanti, A.; Paolo, A. D.; Natale, G.; Tacca, M. D.; Danesi, R. *Eur. J. Pharmacol.* **2006**, *549*, 27−34.
(43) Mueller, S.; Schittenhelm, M.; Honecker, F.; Malenke, E.; Lauber, K.; Wesselborg, S.; Hartmann, J. T.; Bokemeyer, C.; Mayer, F. *Int. J. Oncol.* **2006**, *29*, 471−479.
(44) (a) Billecke, C.; Finniss, S.; Tahash, L.; Miller, C.; Mikkelsen, T.; Farell, N. P.; Bogler, O. *Neuro Oncol.* 2**006**, *8*, 215−226. (b) Yu, C. W.; Li, K. K.; Paug, S. K.; Au-Yeung, S. C.; Ho, Y. P. *Bioorg. Med. Chem. Lett.* **2006**, *16*, 1686−1691.
(45) Desai, D.; Wessling, H. C.; Fisher, R. P.; Morgan, D. O. *Mol. Cell Biol.* **1995**, *15*, 345−350.
(46) Lui, F.; Rothblum-Oviatt, C.; Ryan, C. E.; Piwinica-Worms, H. *Mol. Cell Biol.* **1999**, *19*, 5113−5123.
(47) McGowan, C. H.; Russell, P. *EMBO J.* **1995**, *14*, 2166−2175.
(48) Clarke, P. R.; Leiss, D.; Pagano, M.; Karsenti, E. *EMBO J.* **1992**, *11*, 1751−1761.
(49) Garrett, M. D. *Curr. Sci.* **2001**, *81*, 515−522.
(50) Hagting, A.; Karlsson, C.; Clute, P.; Jackman, M.; Pines, J. *EMBO J.* **1998**, *17*, 4127−4138.
(51) Shimizu, T.; O'Connor, P. M.; Kohn, K. W.; Pommier, Y. *Cancer Res.* **1995**, *5*, 228−231.
(52) Jin, P.; Gu, Y.; Morgan, D. O. *J. Cell Biol.* **1996**, *134*, 963−970.

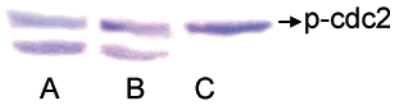

Figure 4. **1b** arrests the cells at the G2 phase of the cell cycle. Western blot of the cell lysate treated with vehicle (A), 10 μM **1b** (B), and 20 μM **1b** (C). Upper band corresponds to the phosphorylated form (p-cdc2), and the lower band corresponds to the unphosphorylated form of the protein cdc2, as independently verified by detecting with monoclonal cdc2 antibody (see Supporting Information, Figure S5).

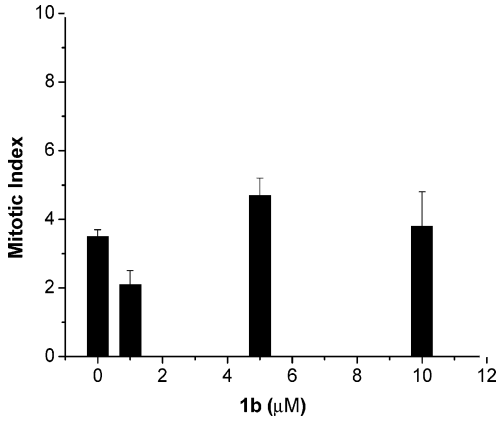

Figure 5. **1b** did not arrest the cells at mitosis. HeLa cells were incubated without or with different concentrations (1, 5, and 10 μM) of **1b** for 24 h, and mitotic cells were visualized after staining the cells with DAPI. Mitotic index was calculated as the percentage of mitotic cells in 1700 cells counted per experiment.

observed, and the protein was evenly distributed in the cell. The results suggested that the inactive cdc2 is not able to form an active complex with cyclin B1 and thereby remains in the cytoplasm and is not translocated to the nucleus, preventing the progression of the cells to mitosis. Further, DAPI staining of the cells treated with different concentrations of **1b** was done to score the mitotic cells. The mitotic index (% of total cells in mitosis) of **1b**-treated cells was similar to that of the untreated cells, which showed that the cells were not arrested in mitosis (Figure 5). Therefore, these results suggest that **1b** causes overexpression of cyclin B1, which arrests the cells at the G2−M transition phase of the cell cycle, and the mitotic entry of the cells is prevented by the inactivation of cdc2 by phosphorylation.

G2 checkpoint targets several signaling pathways, including the p53 pathway, to ensure that cell death follows the G2 arrest.[53] p53 is an important tumor suppressor protein, which is mutated in most of the human cancers. Therefore, we have chosen HCT 116 (human colon adenocarcinoma cells), which has wild-type p53,[54] to study the effect of **1b** on p53 activation. Different stress signals increase the stability of the wild-type p53 and cause the translocation of the protein from the cytoplasm to the nucleus. Nuclear accumulation of p53 results in the transcription of p53-responsive genes, such as p21, bax, etc.[55] p53 plays important roles in the G1 and G2 arrest and induction of apoptosis by the transcriptional activation of its downstream targeted genes.[56] Microscopic analysis of **1b** (20 μM)-treated cells stained with anti-p53 antibody showed that over 69% of cells showed nuclear accumulation of p53, whereas only 11% of the control cells showed nuclear accumulation of p53 (Figure 6). To check whether the downstream targets of p53 are activated upon p53 nuclear accumulation, we stained the HCT cells with antibody against p21 (Figure 7). Nuclear accumulation of p21 was observed in **1b**-treated cells, which was absent in the control cells. The data clearly suggest that nuclear accumulation of p53 resulted in the activation of p53-dependent genes. The results indicate that a p53-dependent pathway is involved in the cell cycle arrest and cell death induced by **1b**.

To elucidate whether **1b** induces apoptotic cell death, apoptotic characteristics of cells incubated with different concentrations (0, 5, and 10 μM) of **1b** for 24 h were studied. Live and dead/apoptotic cells were visualized by propidium iodide staining (Figure 8A). Control cells remained viable after 24 h, as evidenced by the absence of propidium iodide staining. After 24 h of **1b** treatment, cells were stained positive for propidium iodide, indicating that the cells either were in late apoptosis or underwent necrosis. Further condensation/shrinkage of the nucleus associated with apoptosis were seen by DAPI staining (Figure 8B).

Antibacterial activities of the gold (**1c**) and silver (**1d**) complexes were tested by treating *Bacillus subtilis* and *Escherichia coli* with different concentrations of the compounds and measuring the bacterial growth at different time points. **1c** and **1d** inhibited the growth of Gram-positive *B. subtilis* but did not show any effect on the growth of Gram-negative *E. coli*. To verify whether the metal was responsible for the observed activities of **1c** and **1d**, the ligand precursor **1** was also tested for antimicrobial activity. **1** did not inhibit bacterial growth, suggesting that the ligand precursor does not have antibacterial activity. Among the two, the gold complex **1c** was more effective, as it produced over 80% inhibition of *B. subtilis* growth after 12 h incubation. It is worth mentioning that, owing to the greater stability of the gold−NHC bond,[19] the gold complex **1c** is presumably less vulnerable to the biologically active thiol groups than the silver analogue **1d**, thereby accounting for its superior activity (Figure 9). Specifically, for the growth of wild-type *B. subtilis* 168, the half-maximal inhibitory concentration (IC_{50}) and minimum inhibitory concentration (MIC) for **1c** were calculated to be 4 ± 0.8 μM and 15 ± 2.3 μM, respectively. Similarly, the IC_{50} and MIC for **1d** were determined to be 9 ± 1.5 μM and 25 ± 3.2 μM. The inhibitory activity of **1c** is comparable to those of other reported antibacterial agents, such as Dichamanetins (MIC = 1.7 μM),[57] 2‴-hydroxy-5″-benzylisouvarinol-B (MIC = 2.6 μM),[57] Sanguinarine (MIC = 3 μM),[58] and totarol (MIC = 2 μM).[59] In this regard, it is worth mentioning that a few two-coordinated gold complexes of phosphines are reported to exhibit significant antimicrobial activities against the Gram-positive *B. subtilis* bacteria. For example, the reported MIC values in the following complexes are [Au(o-Hpen)(PPh_3)] (o-Hpen = 2-amino-3-

(53) Yu, J.; Zhang, L. *Biochem. Biophys. Res. Commun.* **2005**, *331*, 851−858.
(54) (a) Rahman-Roblick, R.; Roblick, U. J.; Hellman, U.; Conrotto, P.; Liu, T.; Becker, S.; Hirschberg, D.; Jornvall, H.; Auer, G.; Wiman, K. G. *Proc. Natl. Acad. Sci. U.S.A.* **2007**, *104*, 5401−5406. (b) Toscano, F.; Parmentier, B.; Fajoui, Z. E.; Estornes, Y.; Chayvialle, J. A.; Saurin, J. C.; Abello, J. *Biochem. Pharmacol.* **2007**, *74*, 392−406.
(55) Gottifredi, V.; Shieh, S. Y.; Taya, Y.; Prives, C. *Proc. Natl. Acad. Sci. U.S.A.* **2001**, *98*, 1036−1041.
(56) Levine, A. J. *Cell* **1997**, *88*, 323−331.
(57) Urgaonkar, S.; La Pierre, H. S.; Meir, I.; Lund, H.; RayChaudhuri, D.; Shaw, T. J. *Org. Lett.* **2005**, *7*, 5609−5612.
(58) Beuria, T. K.; Santra, M. K.; Panda, D. *Biochemistry* **2005**, *44*, 16584−16593.
(59) Jaiswal, R.; Beuria, T. K.; Mohan, R.; Mahajan, S. K.; Panda, D. *Biochemistry* **2007**, *46*, 4211−4220.

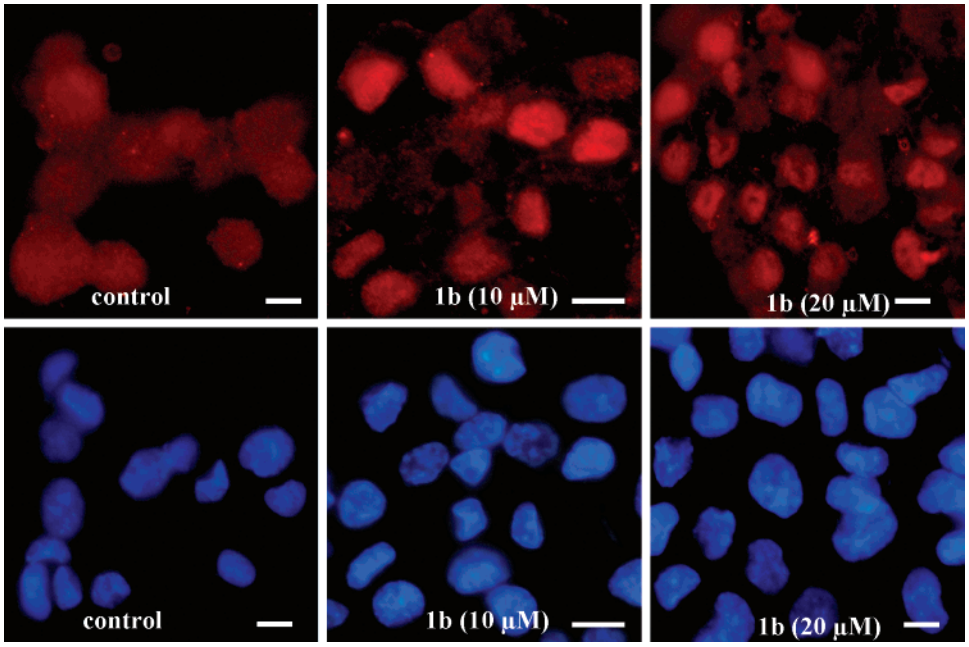

Figure 6. **1b**-induced cell cycle arrest activates the p53 pathway. Immunofluorescence images of HCT 116 cells in the absence and in the presence of 10 and 20 μM **1b** stained with anti-p53 antibody. Upper panels show cells stained with antibody against p53 (red), and the lower panels show DNA of the corresponding cells stained with DAPI (blue). Scale bar represents 10 μm.

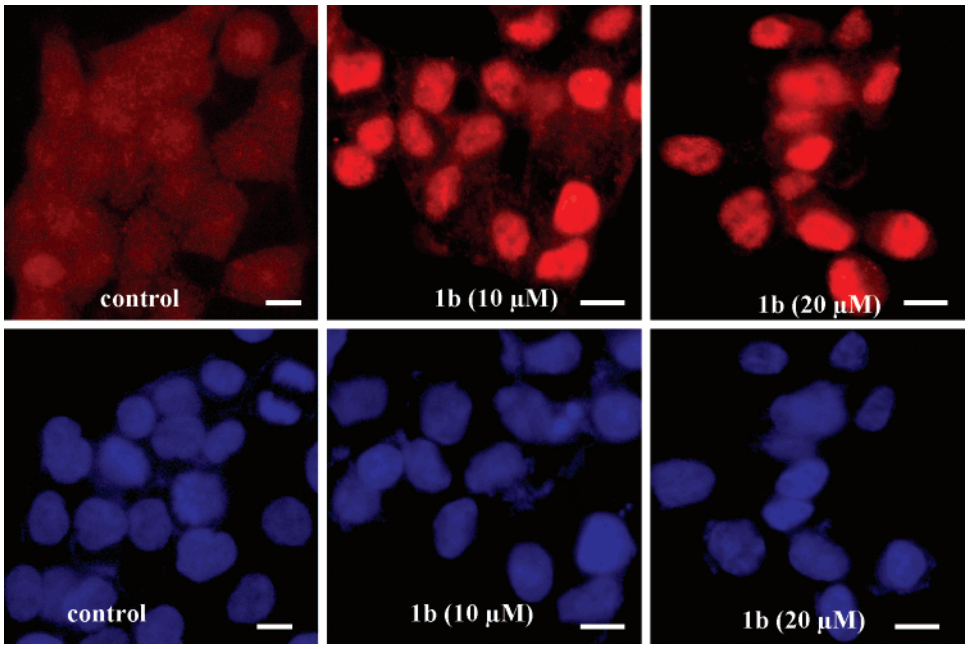

Figure 7. **1b** activates the downstream targets of the p53 pathway. Immunofluorescence images of HCT 116 cells in the absence and in the presence of 10 and 20 μM **1b** stained with anti-p21 antibody. Top panels show cells stained with antibody against p21 (red), and the lower panels show DNA of the corresponding cells stained with Hoescht 33258 (blue). Scale bar represents 10 μm.

mercapto-3-methylbutanoic acid), 31.3 μg mL^{-1};[6c] [Au(2-Hmna)(PPh$_3$)] (2-Hmna = 2-mercaptonicotinic acid), 62.5 μg mL^{-1};[6c] [Au(im)(PPh$_3$)] (im = imidazole), 125 μg mL^{-1};[6d] and [Au(6-Hmna)(PPh$_3$)] (6-Hmna = 6-mercaptonicotinic acid), 500 μg mL^{-1}).[6c] The comparison of the Au−NHC complex **1c** with the Au−phosphine complexes becomes relevant given the fact that both NHCs and phosphines are strong σ-donor ligands[19] and also, in the absence of any other report of Au−NHC complexes showing antimicrobial activity against *B. subtilis* bacteria, a more direct comparison with **1c** is not possible. In the case of silver, its complexes with amino acids like aspartic acid, glycine, and asparagine each gave MIC values of 125 μg mL^{-1} against the *B. subtilis* bacteria.[60] Furthermore, an interesting correlation that emerges out of the Mulliken and natural charge analyses of **1c** and **1d** is that the complex having the more electron-rich metal center, i.e., the gold complex **1c**, showed better antimicrobial activity (see Supporting Information, Table S7).

The morphology of the *B. subtilis* cells was studied after incubating the cells with **1c** and **1d** for 4 h (Figure 10).

(60) Nomiya, K.; Yokoyama, H. *J. Chem. Soc., Dalton Trans.* **2002**, 2483−2490.

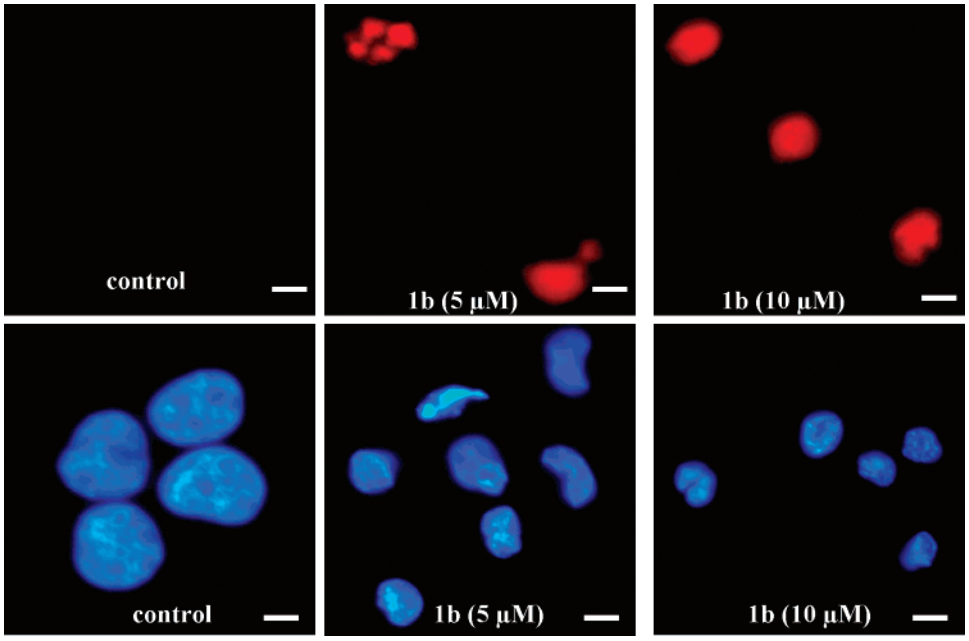

Figure 8. **1b** induces HeLa cell death. Cells were incubated with different concentrations (0, 5, and 10 μM) of **1b** for 24 h. (A) Live and dead cells were visualized after staining the cells with propidium iodide (red). (B) Nuclear morphology was studied after staining the cells with DAPI (blue). Scale bar represents 10 μm.

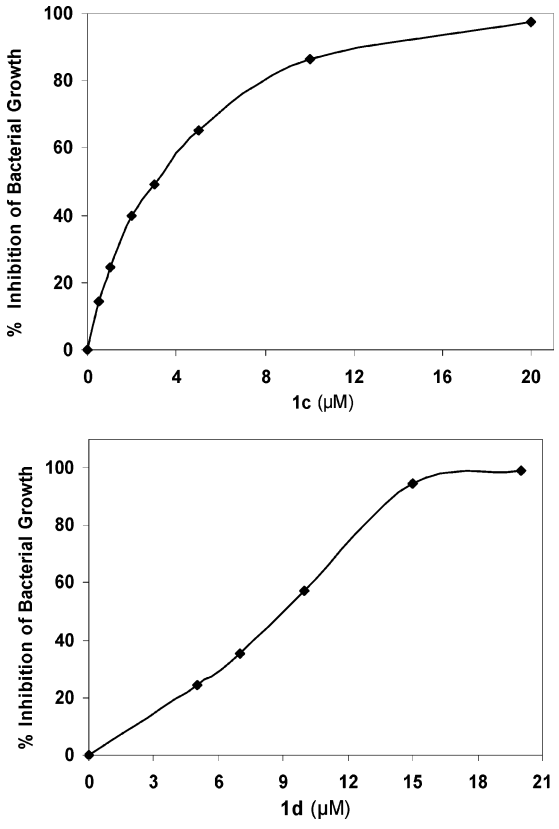

Figure 9. Percent inhibition of *B. subtilis* 168 cell proliferation by **1c** and **1d**.

Incubation of *B. subtilis* cells with 4 μM **1c** for 4 h increased the cell length by 3.5-fold from 2.2 $\pm$ 0.5 μm to 7.3 $\pm$ 3.1 μm relative to the control experiment carried out in the absence of **1c**, indicating that the gold complex **1c** inhibits bacterial proliferation by blocking cytokinesis.[58,59] In contrast, very little increase in cell length was observed in the presence of 10 μM **1d**. The mean length of *B. subtilis* cells was determined to be 3.4 $\pm$ 0.8 μm in the presence of 10 μM **1d**.

Conclusion

In summary, specially designed Pd complexes of the types (NHC)Pd(pyridine)Cl_2 (**1a**) and $(NHC)_2PdCl_2$ (**1b**) have been found to exhibit potent anticancer activity, while the Ag and Au complexes, (NHC)MCl [M = Au, **1c**; Ag, **1d**], display significant antimicrobial activities. In particular, **1b** inhibited proliferation of HeLa, MCF-7, and HCT 116 cells in culture at low micromolar concentrations, which was found to be considerably stronger than the inhibitory concentration of the benchmark drug, cisplatin. The mode of action of **1b** involves arresting the cells at the G2 phase, thereby preventing the mitotic entry of the cells. The blocked cells underwent cell death by a p53-dependent pathway.

Experimental Section

General Procedures. All manipulations were carried out using a combination of glovebox and standard Schlenk techniques. Solvents were purified and degassed by standard procedures. 1-Benzyl-3-*tert*-butylimidazolium chloride[34] was prepared according to a modified literature procedure. ^{1}H and ^{13}C{^{1}H} NMR spectra were recorded on a Varian 400 MHz NMR spectrometer. ^{1}H and ^{13}C NMR peaks are labeled as singlet (s), doublet (d), triplet (t), multiplet (m), and septet (sept). Infrared spectra were recorded on a Perkin-Elmer Spectrum One FT-IR spectrometer. X-ray diffraction data for compounds **1a**−**d** were collected on a Bruker P4 diffractometer equipped with a SMART CCD detector (see Supporting Information, Table S1). The structures were solved using direct methods and standard difference map techniques and were refined by full-matrix least-squares procedures on F^2 with SHELXTL (version 6.10).

Synthesis of [1-Benzyl-3-*tert*-butylimidazol-2-ylidene]AgCl (1d). 1-Benzyl-3-*tert*-butylimidazolium chloride (2.00 g, 8.00 mmol) and Ag_2O (0.924 g, 4.00 mmol) were taken in dichloromethane (ca. 50 mL), and the mixture was stirred at room temperature for 4 h. It was then filtered, solvent was removed from the filtrate, and the off-white sticky product **1d** was dried under vacuum (1.33 g, 46%). The metal

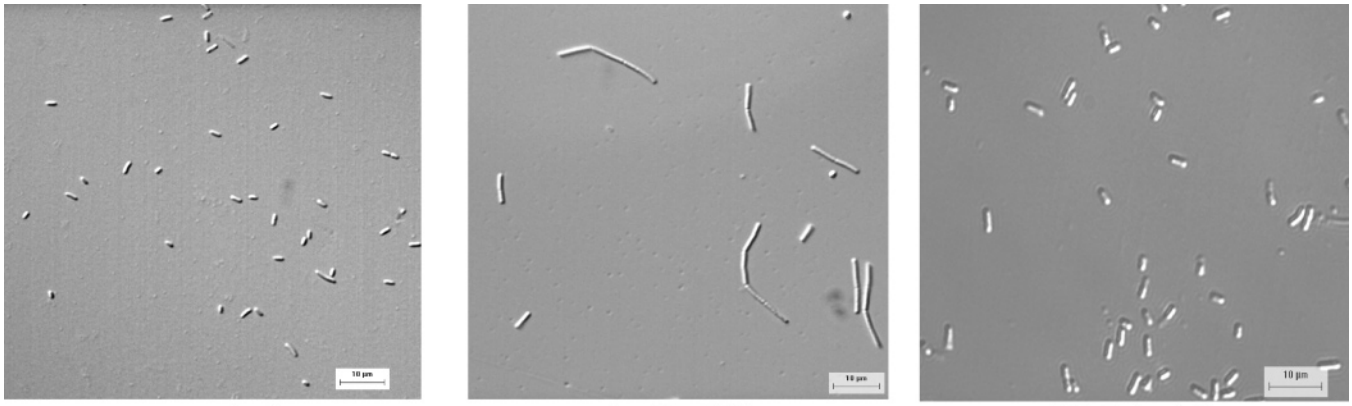

Figure 10. Effects of **1c** and **1d** on the morphology of *B. subtilis*. Cells were incubated for 4 h in the absence and in the presence of **1c** and **1d**, and the cell morphology was visualized by DIC microscopy. Scale bar represents 10 μm.

complex was crystallized from acetonitrile employing slow-evaporation technique and was used for biological studies. ^{1}H NMR ($CDCl_3$, 400 MHz, 25 °C): δ 7.37−7.33 (m, 3H, C_6H_5), 7.24 (br, 2H, C_6H_5), 7.17 (s, 1H, NC*H*CHN), 6.90 (s, 1H, NCHC*H*N), 5.34 (s, 2H, CH_2), 1.74 (s, 9H, CH_3). ^{13}C NMR ($CDCl_3$, 100 MHz, 25 °C): δ 177.7 (N*C*N), 135.4 (*ipso*-C_6H_5), 129.0 (*o*-C_6H_5), 128.5 (*m*-C_6H_5), 127.6 (*p*-C_6H_5), 119.5 (N*C*HCHN), 119.4 (NCH*C*HN), 57.8 (*C*(CH_3)$_3$), 56.7 (*C*H_2), 31.7 (C(*C*H_3)$_3$). IR (Nujol): 2858 (s), 2375 (w), 1557 (w), 1458 (s), 1375 (m), 1310 (w), 1220 (w), 1032 (w), 728 (w) cm^{-1}. Anal. Calcd for $C_{14}H_{18}AgClN_2\cdot(CH_2Cl_2)$: C, 40.71; H, 4.56; N, 6.33. Found: C, 40.77; H, 4.74; N, 5.84.

Synthesis of [1-Benzyl-3-*tert*-butylimidazol-2-ylidene]AuCl (1c). A mixture of [1-benzyl-3-*tert*-butylimidazol-2-ylidene]AgCl (**1d**, 0.358 g, 1.00 mmol) and (SMe_2)AuCl (0.297 g, 1.00 mmol) was taken in dichloromethane (ca. 30 mL) and stirred at room temperature for 5 h. It was then filtered, and the solvent was removed from the filtrate under vacuum to obtain an off-white sticky product, **1c** (0.137 g, 31% yield). The metal complex was crystallized from acetonitrile employing slow-evaporation technique and was used for biological studies. ^{1}H NMR ($CDCl_3$, 400 MHz, 25 °C): δ 7.35−7.33 (m, 5H, C_6H_5), 7.10 (s, 1H, NC*H*CHN), 6.84 (s, 1H, NCHC*H*N), 5.48 (s, 2H, CH_2), 1.86 (s, 9H, CH_3). ^{13}C NMR ($CDCl_3$, 100 MHz, 25 °C): δ 169.2 (N*C*N), 135.0 (*ipso*-C_6H_5), 128.8 (*o*-C_6H_5), 128.4 (*m*-C_6H_5), 127.9 (*p*-C_6H_5), 119.0 (N*C*HCHN), 118.5 (NCH*C*HN), 58.8 (*C*(CH_3)$_3$), 56.2 (*C*H_2), 31.5 (C(*C*H_3)$_3$). IR (Nujol): 3171 (w), 2857 (s), 2723 (w), 2375 (w), 1562 (w), 1459 (s), 1375 (m), 1216 (m), 725 (m), 633 (w) cm^{-1}. HRMS (ES): *m*/*z* 411.1143 [(NHC)Au]$^+$, calcd 411.1136. Anal. Calcd for $C_{14}H_{18}AuClN_2$: C, 37.64; H, 4.06; N, 6.27. Found: C, 37.99; H, 3.50; N, 6.29.

Synthesis of *trans*-[1-Benzyl-3-*tert*-butylimidazol-2-ylidene]Pd(pyridine)Cl_2 (1a). A mixture of 1-benzyl-3-*tert*-butylimidazolium chloride (0.194 g, 0.775 mmol), $PdCl_2$ (0.150 g, 0.845 mmol), and K_2CO_3 (0.161 g, 1.61 mmol) was refluxed in pyridine (ca. 4 mL) for 16 h. The reaction mixture was filtered, and the solvent was removed under vacuum. The residue was then washed with aqueous $CuSO_4$ solution, and the aqueous layer was extracted with chloroform (ca. 3 × 10 mL). The organic layer was collected, and the solvent was removed under vacuum to obtain a yellow solid, **1a** (0.049 g, 14%). The metal complex was crystallized from acetonitrile employing slow-evaporation technique and was used for biological studies. ^{1}H NMR ($CDCl_3$, 400 MHz, 25 °C): δ 9.01 (d, 2H, $^3J_{HH}$ = 8 Hz, *o*-NC_5H_5), 7.76 (t, 1H, $^3J_{HH}$ = 8 Hz, *p*-NC_5H_5), 7.54 (t, 2H, $^3J_{HH}$ = 8 Hz, *m*-NC_5H_5), 7.39−7.35 (m, 5H, C_6H_5), 7.07 (br, 1H, NCHC*H*N), 6.70 (br, 1H, NC*H*CHN), 6.16 (s, 2H, CH_2), 2.12 (s, 9H, C(CH_3)$_3$). ^{13}C{^{1}H} NMR ($CDCl_3$, 100 MHz, 25 °C): δ 151.4 (N*C*N−Pd), 146.3 (*o*-NC_5H_5), 137.9 (*ipso*-C_6H_5), 135.2 (*p*-NC_5H_5), 129.3 (*o*-C_6H_5), 128.9 (*m*-C_6H_5), 128.5 (*p*-C_6H_5), 124.4 (*m*-NC_5H_5), 120.5 (NCH*C*HN), 120.4 (N*C*HCHN), 59.1 (*C*(CH_3)$_3$), 56.1 (*C*H_2), 32.1 (C(*C*H_3)$_3$). IR (Nujol): 2723 (w), 1651 (w), 1595 (w), 1457 (s), 1375 (s), 1206 (m), 1149 (m), 1100 (m), 1062 (m), 807 (w), 768 (m), 694 (m) cm^{-1}. Anal. Calcd for $C_{19}H_{23}Cl_2N_3Pd$: C, 48.48; H, 4.92; N, 8.93. Found: C, 48.83; H, 4.44; N, 8.97.

Synthesis of [1-Benzyl-3-*tert*-butylimidazol-2-ylidene]$_2$PdCl$_2$ (1b). [1-Benzyl-3-*tert*-butylimidazol-2-ylidene]AgCl **(1d**, 0.354 g, 1.00 mmol) and Pd(COD)Cl_2 (0.143 g, 0.500 mmol) were dissolved in acetonitrile (ca. 30 mL), and the mixture was refluxed for 6 h and then cooled. The solvent was reduced to ca. 3 mL, and the mixture was kept overnight. Light yellow crystalline product **1b** was obtained, which was filtered, washed with acetonitrile (ca. 5 mL), and dried under vacuum (0.089 g, 29%). The metal complex was crystallized from acetonitrile employing slow-evaporation technique and was used for biological studies. ^{1}H NMR ($CDCl_3$, 400 MHz, 25 °C): δ 7.54 (d, 2H, $^3J_{HH}$ = 8 Hz, *o*-C_6H_5), 7.40 (t, 2H, *m*-C_6H_5), 7.35 (t, 1H, *p*-C_6H_5), 7.00 (s, 1H, NC*H*CHN), 6.63 (s, 1H, NCHC*H*N), 6.17 (s, 2H, CH_2), 1.98 (s, 9H, CH_3). ^{13}C NMR ($CDCl_3$, 100 MHz, 25 °C): δ 166.9 (N*C*N), 136.0 (*ipso*-C_6H_5), 129.0 (*o*-C_6H_5), 128.8 (*m*-C_6H_5), 128.1 (*p*-C_6H_5), 119.6 (N*C*HCHN), 119.6 (NCH*C*HN), 58.6 (*C*(CH_3)$_3$), 55.5 (*C*H_2), 32.0 (C(*C*H_3)$_3$). IR (Nujol): 2859 (s), 2378 (w), 1562 (w), 1458 (m), 1376 (m), 1221 (m), 1030 (m), 825 (w), 723 (m) cm^{-1}. HRMS (ES): *m*/*z* 569.1659 [(NHC)$_2$PdCl]$^+$, calcd 569.1663. Anal. Calcd for $C_{28}H_{36}Cl_2N_4Pd$: C, 55.50; H, 5.99; N, 9.25. Found: C, 55.77; H, 5.78; N, 9.49.

Antitumor Studies. 1. Reagents. Sulforhodamine B (SRB), alkaline phosphatase (ALP)-conjugated anti-mouse or anti-rabbit IgG, bovine serum albumin (BSA), Hoechst 33258, and cisplatin (*cis*-diammineplatinum(II) dichloride) were purchased from Sigma (St. Louis, MO). Anti-mouse IgG-alexa 568 conjugate and 4′,6-diamidino-2-phenylindole (DAPI) were purchased from Molecular Probes (Eugene, OR). Mouse monoclonal anti-p53 antibody, mouse monoclonal anti-p21 antibody, and mouse monoclonal anti-cyclin B1 antibody were from Santa Cruz, and rabbit polyclonal phospho-cdc2 Tyr 15 antibody was obtained from Novus Biologicals. Mouse monoclonal anti-cdc2 antibody was obtained from Cell Signaling Technology. All other reagents used were of analytical grade.

2. Cell Culture. Human cervical carcinoma cells (HeLa), human breast cancer cells (MCF-7), and human colon adenocarcinoma cells (HCT 116) were cultured in Eagle's Minimal Essential Medium (MEM) and Dulbecco's Modified Eagle's Medium (DMEM), respectively, supplemented with 10% fetal calf serum, 1.5 g/L sodium bicarbonate, and 1% antibiotic−antimycotic solution containing streptomycin, amphoterecin B, and penicillin. Cells were maintained at 37 °C in a humidified atmosphere of 5% carbon dioxide and 95% air. For cell proliferation assays, cells were seeded at a density of 1 × 10^5 cells/mL on 96-well plates. For immunofluorescence studies, 0.6 × 10^5 cells/mL were grown as a monolayer on glass coverslips. Compounds diluted

in dimethyl sulfoxide (DMSO, 0.1% final concentration) were added to the culture medium 24 h after seeding.

3. Cell Proliferation Assay. The effects of cisplatin and **1a**−**d** on the proliferation of three different cancer cells (HeLa, MCF-7, and HCT 116) after one cell cycle were determined using sulforhodamine B assay as described previously.[61,62] Briefly, 1×10^5 cells/mL were seeded in each well in 96-well plates for 24 h and then incubated without or with different concentrations of these agents at 37 °C for 24, 48, and 16 h for HeLa, MCF-7, and HCT 116 cells, respectively. In order to compare the potency of **1b** with that of cisplatin, the cells were treated with the compounds and the assay was performed simultaneously with the two compounds. After incubation of cells with the compounds for one cell cycle, cell growth was stopped by the addition of 10% trichloroacetic acid and stained with 0.4% sulforhodamine B dissolved in 1% acetic acid. Unbound dye was removed by washing with 1% acetic acid, and the protein content was determined by measuring absorbance at 560 nm in a Bio-Rad model 680 microplate reader after extracting with 10 mM Tris base.[61] Data are the averages of three independent experiments (Tables 1 and 2). IC_{50} was calculated as the concentration of the compound that inhibited the proliferation of cells by 50% relative to the untreated control cells.

4. Immunofluorescence Microscopy. Cells (0.6×10^5 cells/mL) seeded on glass coverslips were exposed to different concentrations of **1b** or cisplatin for one cell cycle at 37 °C. Cells were fixed in 3.7% formaldehyde and permeabilized with ice-cold methanol for 10 min at −20 °C. After blocking of nonspecific sites with 2% BSA, cells were stained with mouse monoclonal anti-p53 antibody (1:300 dilution in 2% BSA), mouse monoclonal anti-p21 antibody (1:300 dilution in 2% BSA), or mouse monoclonal anti-cyclin B1 antibody (1:300 dilution in 2% BSA) for 2 h at 37 °C, followed by Alexa 568-conjugated sheep anti-mouse IgG antibody (1:400 dilution in 2% BSA) for 1 h at 37 °C. To visualize DNA, cells were stained with 1 μg/mL DAPI for 20 s or Hoechst 33258 for 10 min. Cells were washed with 1 × PBS after all incubations. All the coverslips were mounted in 50% glycerol in PBS containing 5 mM 1,4-diazabicyclo[2.2.2]octane , the cells were examined with a Nikon Eclipse 2000-U fluorescence microscope, and the images were analyzed with Image-Pro Plus software[62] (Figures 3, 5−8).

5. Annexin V/Propidium Iodide Staining. HeLa cells were plated at a density of 6×10^4 cells/mL and grown in 24-well tissue culture plates 24 h before the addition of **1b**. Cells were then grown in the absence and in the presence of different concentrations of **1b** for an additional 24 h. Subsequently, cells were spun at 2400 rpm for 10 min, and the cells were stained using the Annexin V apoptosis kit (Santa Cruz). Cells were washed twice in PBS and once in 1× assay buffer. To ∼300 μL of the buffer in each well were added 1.5 μL of the Annexin-V FITC and 10 μL of propidium iodide, and the mixture was incubated for 15 min in the dark at room temperature. After 15 min, cells were washed in 500 μL of PBS. The coverslips were mounted and observed immediately using a Nikon Eclipse 2000-U fluorescence microscope, and the images were analyzed with Image-Pro Plus software (Figure 8A). Absence of annexin V and propidium iodide staining denotes viable cells, whereas cells stained positive for annexin V alone are early apoptotic cells. Cells stained positive for both annexin V and propidium iodide indicate late apoptotic cells, and those stained positive for propidium iodide alone are dead cells, which underwent apoptosis or necrosis.

6. Preparation of Cell Lysate and Western Blot Analysis. HeLa cells were seeded at 1.5×10^5 cells/mL in tissue culture flasks. When the cells had grown to 70% confluency, the medium was removed. Fresh media containing different concentrations of **1b** were added and incubated for an additional 24 h. Both the floating and attached cells were harvested with the help of a cell scrapper and collected by centrifugation. The cells were washed thrice in PBS, and the cell lysate was extracted at 4 °C using lysis buffer (50 mM Tris, pH 7.4, 150 mM NaCl, 0.1% Triton X-100, 0.2% Nonidet P-40, 4 mM EDTA, 50 mM NaF, 1 mM DTT) containing protease inhibitors. The lysed cell suspension was centrifuged at 1200*g* for 10 min, and the resulting supernatants were used as cell lysate.

The protein concentration of the cell lysate was determined by Bradford assay.[63] An equal amount (50 μg) of each sample was separated by SDS−PAGE (10% acrylamide gel) and electroblotted onto a poly(vinylidene difluoride) (PVDF) membrane (Amersham). The blot was blocked with Tris-buffered saline containing 0.05% Tween 20 (TBST) and 5% non-fat skim milk for 12 h at room temperature. The blots were independently probed with rabbit polyclonal anti-phosphor-cdc2 antibody (1:1200) and mouse monoclonal cdc2 antibody (1:1200) for 2 h. The blot was washed thrice with TBST and incubated with alkaline phosphatase-conjugated secondary antibodies (1:5000) for 1 h at room temperature. After three washes with TBST, the membrane was developed using 5-bromo-4-chloro-3-indolyl phosphate/nitro blue tetrazolium (BCIP/NBT) substrate.

Antimicrobial Studies. 1. Screening the Effects of Different Compounds on *Bacillus subtilis* 168 Strain. Wild-type *B. subtilis* cells and *E. coli* cells were grown in Luria-Broth (LB) media in the presence of different concentrations (0, 0.5, 1, 5, 10, and 25 μM) of **1c** and **1d** for different time intervals (0, 4, 8, and 12 h). The inhibition of bacterial growth was monitored by recording the absorbance of the bacterial culture at 600 nm using a JASCO V-530 spectrophotometer at the above-mentioned time intervals. The compounds **1c** and **1d** did not affect growth of *E. coli* cells.

2. Effects of 1c and 1d on the Morphology of *B. subtilis* Cells. *B. subtilis* cells were inoculated in LB media containing 4 μM **1c** and 10 μM **1d**, and the cells were grown at 37 °C for 4 h. After the bacterial cells were fixed with 0.04% glutaraldehyde and 2.5% formaldehyde, cells were harvested and resuspended in 100 μL of PBS. A 5 μL aliquot of the suspension was placed on a clean coverslip, and the morphology of the bacterial cells was examined using diffraction interference contrast (DIC) microscopy. The images were analyzed with Image-Pro Plus software (Figure 9).

3. Determination of MIC and IC_{50} of 1c and 1d against *B. subtilis* 168. Wild-type *B. subtilis* 168 cells grown overnight in LB medium were used to determine the MIC and IC_{50} of both compounds **1c** and **1d**. *B. subtilis* 168 cells were grown in the absence and in the presence of different concentrations of **1c** and **1d** in LB media for 5 h and LB-agar plates overnight, respectively. The inhibitory effects of both compounds were monitored by measuring the absorbance at 600 nm (A_{600}) and counting the colonies of the *B. subtilis* 168 cells on the LB-agar plates. The half-maximum inhibitory concentration (IC_{50}) was determined by plotting the percent inhibition of bacterial growth against different concentrations (1−20 μM) of both compounds. The minimum inhibitory concentration (MIC) was determined by counting the number of colonies of *B. subtilis* 168 cells in the absence and in the presence of different concentrations (2−20 μM) of both compounds in the LB-agar Petri plates (Figure 10).

Computational Methods. Density functional theory calculations were performed on the four transition metal complexes of NHCs, namely, *trans*-[1-benzyl-3-*tert*-butylimidazol-2-ylidene]Pd(pyridine)-Cl_2 (**1a**), [1-benzyl-3-*tert*-butylimidazol-2-ylidene]$_2$$PdCl_2$ (**1b**), [1-benzyl-3-*tert*-butylimidazol-2-ylidene]AuCl (**1c**), and [1-benzyl-3-*tert*-butylimidazol-2-ylidene]AgCl (**1d**), using the Gaussian 03[64] suite of quantum chemical programs. Specifically, single-point calculations were performed on the complexes **1a**−**d** using atomic coordinates obtained from X-ray analysis. The Becke three-parameter exchange functional, in conjunction with the Lee−Yang−Parr correlation

(61) Papazisis, K. T.; Geromichalos, G. D.; Dimitriadis, K. A.; Kortsaris, A. H. *J. Immun. Methods* **1997**, *208*, 151−158.
(62) Mohan, R.; Banerjee, M.; Ray, A.; Manna, T.; Wilson, L.; Owa, T.; Bhattacharyya, B.; Panda, D. *Biochemistry* **2006**, *45*, 5440−5449.
(63) Bradford, M. M. *Anal. Biochem.* **1976**, *72*, 248−254.
(64) Frisch, M. J.; et al. *Gaussian 03*, Revision C.02; Gaussian, Inc.: Wallingford, CT, 2004.

functional (B3LYP), was employed in this study.[65,66] The Stuttgart−Dresden effective core potential (ECP), representing 19 core electrons, along with valence basis sets (SDD) was used for palladium.[67] All other atoms are treated with 6-31G(d) basis set.[68] All stationary points were characterized as minima by evaluating Hessian indices on the respective potential energy surfaces. Tight SCF convergence (10^{-8} au) was used for all calculations. Natural bond orbital analysis was performed using the NBO3.1 program as implemented in Gaussian 03.[69]

(65) Becke, A. D. *Phys. Rev. A* **1998**, *38*, 3098−3100.
(66) Lee, C.; Yang, W.; Parr, R. G. *Phys. Rev. B* **1988**, *38*, 785−789.
(67) (a) Pang, K.; Quan, S. M.; Parkin, G. *Chem. Commun.* **2006**, 5015−5016. (b) Yang, G.; Jin, C.; Hong, J.; Guo, Z.; Zhu, L. *Spectrochim. Acta, Part A* **2004**, *60*, 493−509. (c) Zhang, Y.; Zhang, L.; Tao, H.; Sun, X.; Zhu, L. *Spectrochim. Acta, Part A* **2003**, *59*, 3187−3195.
(68) Hehre, W. J.; Ditchfield, R.; Pople, J. A. *J. Chem. Phys.* **1972**, *56*, 2257−2261.
(69) Reed, A. E.; Curtiss, L. A.; Weinhold, F. *Chem. Rev*. **1988**, *88*, 899−926.

Acknowledgment. Financial support for this work was provided by Department of Science and Technology. We are grateful to the National Single Cystal X-ray Diffraction Facility at IIT Bombay, India, for the crystallographic results. D.P. is a Swarnajayanti Fellow. S.R., R.M., J.K.S., and M.K.S. thank CSIR-UGC, India, for research fellow ships.

Supporting Information Available: Crystallographic information for **1a**−**d** (CIF), B3LYP coordinates of single-point calculations of **1a**−**d**, Mulliken and natural charge analysis data, and complete ref 64. This material is available free of charge via the Internet at http://pubs.acs.org.

JA075889Z